



This discussion paper is/has been under review for the journal Atmospheric Measurement Techniques (AMT). Please refer to the corresponding final paper in AMT if available.

Cross-validation of IASI/MetOp derived tropospheric δD with TES and ground-based FTIR observations

J.-L. Lacour¹, L. Clarisse¹, J. Worden², M. Schneider³, S. Barthlott³, F. Hase³,
C. Risi⁴, C. Clerbaux^{1,5}, D. Hurtmans¹, and P.-F. Coheur¹

¹Spectroscopie de l'Atmosphère, Service de Chimie Quantique et Photophysique, Université Libre de Bruxelles, Brussel, Belgium

²Jet Propulsion Laboratory, California Institute of Technology, Pasadena, California, USA

³Institute for Meteorology and Climate Research (IMK-ASF), Karlsruhe Institute of Technology, Karlsruhe, Germany

⁴UPMC Univ. Paris 06; UMR8539, CNRS/INSU, LMD-IPSL, Paris, France

⁵UPMC Univ. Paris 06; Université Versailles St-Quentin, CNRS/INSU, LATMOS-IPSL, Paris, France

Received: 2 October 2014 – Accepted: 21 October 2014 – Published: 12 November 2014

Correspondence to: J.-L. Lacour (jlacour@ulb.ac.be)

Published by Copernicus Publications on behalf of the European Geosciences Union.

Title Page

Abstract

Introduction

Conclusions

References

Tables

Figures



Back

Close

Full Screen / Esc

Printer-friendly Version

Interactive Discussion



Abstract

The Infrared Atmospheric Sounding Interferometer (IASI) flying on-board MetOpA and MetOpB is able to capture fine isotopic variations of the HDO to H₂O ratio (δD) in the troposphere. Such observations at the high spatio temporal resolution of the sounder are of great interest to improve our understanding of the mechanisms controlling humidity in the troposphere. In this study we aim to empirically assess the validity of our error estimation previously evaluated theoretically. To achieve this, we compare IASI δD retrieved profiles with other available profiles of δD , from the TES infrared sounder onboard AURA and from three ground-based FTIR stations produced within the MUSICA project: the NDACC (Network for the Detection of Atmospheric Composition Change) sites Kiruna and Izana, and the TCCON site Karlsruhe, which in addition to near-infrared TCCON spectra also records mid-infrared spectra. We describe the achievable level of agreement between the different retrievals and show that these theoretical errors are in good agreement with empirical differences. The comparisons are made at different locations from tropical to Arctic latitudes, above sea and above land. Generally IASI and TES are similarly sensitive to δD in the free troposphere which allows to compare their measurements directly. At tropical latitudes where IASI's sensitivity is lower than that of TES, we show that the agreement improves when taking into account the sensitivity of IASI in the TES retrieval. For the comparison IASI-FTIR only direct comparisons are performed because of similar sensitivities. We identify a quasi negligible bias in the free troposphere (-3%) between IASI retrieved δD with the TES one, which are bias corrected, but an important with the ground-based FTIR reaching -47% . We also suggest that model-satellite observations comparisons could be optimized with IASI thanks to its high spatial and temporal sampling.

Cross-validation of IASI/MetOp δD retrievals

J.-L. Lacour et al.

Title Page

Abstract

Introduction

Conclusions

References

Tables

Figures



Back

Close

Full Screen / Esc

Printer-friendly Version

Interactive Discussion



1 Introduction

Water vapour in the troposphere has a central role in the climate system (Pierrehumbert et al., 2007; Sherwood et al., 2010). Yet there are important uncertainties associated with the mechanisms controlling tropospheric water vapour distribution throughout the globe, leading to systematic biases in actual representations (Soden and Bretherton, 1994; Brogniez and Pierrehumbert, 2007; Allan et al., 2003; Bates and Jackson, 1997; Pierce et al., 2006) and an important spread in future climate predictions (Soden and Held, 2006; de Forster and Collins, 2004). In particular, the cloud feedback is responsible for most of the spread in the different climate models (Cess et al., 1990; Dufresne and Bony, 2008) because of the various representations of associated processes in the different models. Recently, Sherwood et al. (2014) showed that, among 43 climate models, the different ways of simulating convective mixing between the lower and middle tropical troposphere was responsible of about half of the variance in climate sensitivity. It is thus crucial to improve representation of hydrological processes.

Observations of water vapour isotopologues have the potential to reveal information on the processes controlling humidity. The different water isotopologues are indeed characterized by distinct vapour pressures and are therefore sensitive to phase changes: the heavy isotopologues (H_2^{18}O , HDO) preferentially condense while the light (H_2^{16}O) preferentially evaporates. Hence, the heavy to light isotopologue ratio provides useful information on the air mass history and can be used to constrain hydrological processes (Strong et al., 2007; Worden et al., 2007; Samuels-Crow et al., 2014; Risi et al., 2012a, b; Noone, 2012). The ratio is commonly expressed in δ notation:

$$\delta D = 1000 \left(\frac{\frac{\text{HDO}}{\text{H}_2\text{O}}}{\text{VSMOW}} - 1 \right), \quad (1)$$

where VSMOW (Vienna Standard Mean Ocean Water) is the reference standard for water isotope ratios (Craig, 1961).

Title Page

Abstract

Introduction

Conclusions

References

Tables

Figures



Back

Close

Full Screen / Esc

Printer-friendly Version

Interactive Discussion



**Cross-validation of
IASI/MetOp δD
retrievals**

J.-L. Lacour et al.

Title Page

Abstract

Introduction

Conclusions

References

Tables

Figures



Back

Close

Full Screen / Esc

Printer-friendly Version

Interactive Discussion



Among the different methods to determine the isotopic composition of water vapour, it has been shown that remote sensing instruments can be used to infer estimates of δD at a sufficient precision for scientific applications (Risi et al., 2012b), with the advantage that they provide measurements over regions and at altitudes that are not easily accessible. Space sounders also have the potential to provide global distributions (Worden et al., 2007; Frankenberg et al., 2009, 2013; Boesch et al., 2013). The Infrared Atmospheric Sounding Interferometer (IASI) (Clerbaux et al., 2009) onboard the MetOp meteorological satellite is particularly suited for measuring δD owing to its unique sampling characteristics (Schneider and Hase, 2011; Lacour et al., 2012). Indeed, IASI samples the atmosphere almost everywhere on the globe two times a day with a ground pixel size of 12 km at nadir.

Because of their inherent lack of vertical sensitivity, measurements derived from remote sounding instruments constitute a more or less complicated function of the quantity of the interest (Rodgers and Connor, 2003) and can not be regarded as true values. The regularization procedure used in the retrievals is in fact often such that they constitute the most probable estimate given the measurement and some a priori statistical information. Moreover retrieved quantities depend also on several parameters of the inversion such as the a priori, the spectroscopic line database, the spectral range etc. For all these reasons, the validity of quantities derived from remote sensing instruments always needs to be evaluated against other observations. It is at the same time crucial to document how different remote sensing products compare between them. In this paper we assess the validity of δD vertical profiles retrieved from IASI at ULB by comparing them with other available profiles of δD in the troposphere. We use the term “cross-validation” according to von Clarmann (2006) for this exercise as we compare IASI vertical profiles against profiles from other remote sounding instruments which do not constitute absolute values of the state of the atmosphere. Our study is similar to the recent cross-validation of IASI δD retrievals from KIT with ground-based FTIRs (Wiegele et al., 2014). We note that there has been recently an increasing number of absolute measurements of tropospheric δD (Schneider et al., 2014; Herman et al., 2014), which

**Cross-validation of
IASI/MetOp δD
retrievals**

J.-L. Lacour et al.

Title Page

Abstract

Introduction

Conclusions

References

Tables

Figures



Back

Close

Full Screen / Esc

Printer-friendly Version

Interactive Discussion



will be essential to validate δD profiles retrieved from the remote sounders and thus to ensure the optimal use of the latter which are for now often limited to relative variations analyses (Risi et al., 2012b). In this study, although we do not use the absolute measurements, we perform the cross-validation with respect to instruments which have been evaluated against them. This allows us to infer some preliminary conclusions on how our retrievals would compare to these references.

We use for the cross-validation of IASI, δD profiles from the TES instrument on-board Aura (Worden et al., 2012) and from ground-based FTIRs from the MUSICA network (Schneider et al., 2012) which are both sensitive to δD in the same part of the troposphere as IASI. We do not perform the comparison with other space sounders, which provide δD retrievals in the upper troposphere or near the surface where IASI is generally less sensitive (Lacour et al., 2012; Schneider and Hase, 2011).

The main purpose of the cross-validation exercise presented here is to verify that two profiles from two different remote sounding instruments agree within their respective limitations (Rodgers and Connor, 2003) that is to say that the estimated profiles are well characterized by their error and sensitivity matrices. In Sect. 2 we introduce the methodology employed to adequately intercompare the different instrument products. Specifics of the δD retrievals (also referred as HDO / H₂O ratio retrieval) are also documented in this section. We then give a brief overview of the different instruments in Sect. 3. In Sects. 4 and 5 we detail the results of the comparison between IASI and TES and between IASI and the ground-based FTIRs respectively.

2 Methodology to inter compare δD profiles

In this study we mainly follow the Rodgers and Connor (2003) methodology developed to inter-compare indirect measurements. Its application to δD retrievals is described below.

2.1 Retrieval of the HDO / H₂O ratio

Retrieving the HDO / H₂O ratio at a sufficient quality from remote sounding instruments is challenging since the retrieval needs to be precise enough to capture the fine isotopic variations and sensitive over the large dynamical range of water vapour concentrations in the troposphere. This requirement is antagonist with the general formulation of the optimal estimation as the precision of the retrieval highly depends on the applied statistical constraint which itself limits the range of possible states. One way of overcoming this limitation is to introduce an inter constraint between the two water isotopologues and to perform the retrieval on a logarithmic scale (Schneider et al., 2006; Worden et al., 2006). The different retrieval products we use here (Lacour et al., 2012; Worden et al., 2012; Schneider et al., 2012) have been obtained applying this constrained approach. One difficulty introduced by the constrained retrieval is the posterior characterization of the δD profiles as the averaging kernels and error covariance matrices obtained are indeed representative of the retrieved states $\log(H_2O)$ and $\log(HDO)$ and can not be directly applied to δD .

Schneider et al. (2012) have developed an elegant method to characterize the vertical profiles of H₂O and δD for retrievals which constrain the ratio $\log(HDO / H_2O)$. This methods allows to transform the products obtained in the $\{\log(H_2O), \log(HDO)\}$ space into a proxy state $\{\log(\text{humidity}), \delta D\}$. It is then possible to provide proxy error covariance matrices and averaging kernels for the δD profile which in turn facilitates its use for geophysical analyses.

In addition, the method allows for a minimization of the cross dependence of the H₂O retrieval on the δD retrieval and vice versa (Schneider et al., 2012). As retrieved H₂O and δD exhibit different vertical sensitivities (the sensitivity to δD being limited compared to H₂O) and are thus not fully representative of the same air mass, Schneider et al. (2012) recommend to distinguish two types of products. A product (type 1) for an optimal use of H₂O vertical profiles alone and a product (type 2) for consistent H₂O and δD data which are likely to be used together and need to be representative

Cross-validation of IASI/MetOp δD retrievals

J.-L. Lacour et al.

Title Page

Abstract

Introduction

Conclusions

References

Tables

Figures



Back

Close

Full Screen / Esc

Printer-friendly Version

Interactive Discussion



Cross-validation of IASI/MetOp δD retrievals

J.-L. Lacour et al.

Title Page

Abstract

Introduction

Conclusions

References

Tables

Figures

◀

▶

◀

▶

Back

Close

Full Screen / Esc

Printer-friendly Version

Interactive Discussion



of the same air mass. This is achieved by reducing the H_2O profile to the δD retrieval sensitivity. In this paper we use this proxy state (type 2) to characterize δD profiles in terms of averaging kernels and error covariance matrices and all retrievals have therefore been a posteriori corrected to obtain a product of type 2. Specifically, according to Schneider et al. (2012) this is done by:

$$\hat{x}^* = \mathbf{P}^{-1} \mathbf{C} \mathbf{P} (\hat{x} - x_a) + x_a, \quad (2)$$

with x_a the a priori state vector, \hat{x} the estimated state vector $\{\log(H_2O), \log(HDO)\}$ the profiles originally retrieved and \hat{x}^* the corrected state vector $\{\log(H_2O), \log(HDO)\}$ that is used to compute the δD ratio of type 2. For the description of \mathbf{P} and \mathbf{C} matrices we refer to Schneider et al. (2012). These matrices ensure the reduction of vertical sensitivity and resolution of the H_2O profile as well as a correction of the cross dependence. Averaging kernels and error covariance matrices from the different retrievals have all been transformed into the $\{\log(\text{humidity}), \delta D\}$ proxy space.

2.2 Transformation between grids

A cross-validation exercise should compare like with like and consists of applying corrections to make the different retrievals comparable. A first step required for the cross-validation involves the adjustment of the different vertical grids on which the retrievals are performed. The state vectors, the error covariance matrices as well as the averaging kernels matrices need to be represented on the same grids to be comparable. The state vector and the error covariance matrices can be transformed into a coarser or a finer grid. Indeed, following Rodgers (2000) the state vector x on a fine grid is related to a reduce vector z on a coarser grid as:

$$x = \mathbf{W}z + \epsilon_{\mathbf{W}}x \quad (3)$$

with \mathbf{W} the interpolation matrix and $\epsilon_{\mathbf{W}}x$ the error induced by the interpolation (Calisesi et al., 2005). The transformation of the state vector on a fine grid to a state vector on

a coarser grid can be obtained via:

$$z = \mathbf{W}^* x \quad (4)$$

where \mathbf{W}^* is the pseudo inverse matrix of \mathbf{W} . The error covariance matrix can be resampled on the coarser grid as follows:

$$5 \quad \mathbf{S}_z = \mathbf{W}^* \mathbf{S}_x \mathbf{W}^{*T}. \quad (5)$$

For the averaging kernels, the interpolation is more complicated. For example, Calisesi et al. (2005) use also the linear transformation to resample the AVK on different grids as follows:

$$\mathbf{A}_z = \mathbf{W}^* \mathbf{A}_x \mathbf{W}. \quad (6)$$

10 The equation has been used to transform averaging kernels on different grids in the case of retrieved profiles from limb sounders (Ceccherini et al., 2003; Calisesi et al., 2005) which are characterized by high vertical resolution compared to nadir sounders. In our study, as it can be seen in Fig. 1, the IASI grid is coarser than the one used for TES and FTIRs. We aim at representing the other retrievals on the same grid as IASI
15 since extrapolation would lead to additional error. Applying Eq. (6) to TES averaging kernels lead to satisfying interpolated averaging kernels matrices. In the case of the FTIR however, this could not be applied without a significant degradation of the matrix owing to the configuration of levels for the FTIR grid. To have the FTIR AVK on IASI vertical grid we therefore interpolated the eigenvectors of the AVK. First, the FTIR
20 averaging kernels matrix is decomposed into its eigenvectors ($\mathbf{AVK} = \mathbf{VDV}^{-1}$); second the leading eigenvectors are interpolated on IASI grid ($\mathbf{V}' = \mathbf{WV}$); and third, the FTIR averaging kernels are reconstructed with the interpolated eigenvectors but with the eigenvalues corresponding to the original AVK ($\mathbf{AVK}' = \mathbf{V}'\mathbf{D}\mathbf{V}'^{-1}$). The \mathbf{AVK}' obtained is then used for the comparison.

Cross-validation of
IASI/MetOp δD
retrievals

J.-L. Lacour et al.

Title Page

Abstract

Introduction

Conclusions

References

Tables

Figures

◀

▶

◀

▶

Back

Close

Full Screen / Esc

Printer-friendly Version

Interactive Discussion



Cross-validation of IASI/MetOp δD retrievals

J.-L. Lacour et al.

Title Page

Abstract

Introduction

Conclusions

References

Tables

Figures



Back

Close

Full Screen / Esc

Printer-friendly Version

Interactive Discussion



5 difference TES-IASI in the δD profiles and are plotted as green line in Fig. 4. For the direct comparison, we find that the real difference is lower than the expected one below 7 km. This indicates that the difference TES-IASI at these altitudes is in agreement with the theoretical error budget. The fact that the real difference exceeds the expected one

10 above 7 km could be due to an underestimation of the IASI's observational error (since all other contributions are mostly negligible). When smoothing TES retrieved profiles with IASI averaging kernels the real differences decrease in the free troposphere where the smoothing error was important. As for the non-smoothed comparison, the real difference remains below the theoretical one over the entire 0–7 km range.

15 While these figures are indicative of the error budget above the Indian and Pacific Oceans, the variations in sensitivity are such that the budget will depend on humidity and temperature conditions. However, we found that the results presented in Fig. 4 are generally representative of all observations above the oceans. In the following subsection we provide a more statistical view on the agreement between TES and IASI.

4.4.1 Statistics of the agreement between IASI and TES

20 In this subsection we compare IASI to TES statistically for the MD and PIO datasets. We focus on retrieved δD values at 4.5 km which is the altitude where IASI is the most sensitive above the oceans. For the PIO dataset we document the agreement for both the direct and the smoothed comparisons. For the MD dataset we only consider the direct comparison because the sensitivity of TES – depending on the latitude (Fig. 3) – is sometimes higher and sometimes lower than IASI sensitivity. As we discussed in Sect. 4.2 the direct comparison is meaningful since the expected differences are substantially smaller than the natural variability at a global scale. We summarize the results from the comparison between IASI and TES in Table 1, in terms of 1σ SD, slope of the major axis regression (m) and Pearson correlation coefficient (r).

25 For the PIO dataset we found a SD of the difference of 43‰ for the direct comparison which decreases to 35‰ when TES retrievals are smoothed with IASI averaging kernels. These value are in line with the theoretical estimations of the error. The correlation

Cross-validation of IASI/MetOp δD retrievals

J.-L. Lacour et al.

Title Page

Abstract

Introduction

Conclusions

References

Tables

Figures



Back

Close

Full Screen / Esc

Printer-friendly Version

Interactive Discussion



coefficients have values of 0.55 and 0.61 for the direct and smoothed comparison respectively. These values for the correlation are driven by the low signal to noise ratio of the compared quantities. Indeed, we calculated that we would expect a correlation coefficient not larger than 0.7 if we were to compare TES retrieved profiles with the same profiles perturbed by a random noise of 35%. The correlation coefficient found for the IASI-TES comparison is coherent with this and demonstrate that TES and IASI δD co-vary well together. The slopes of the regression curves indicate that the TES variability is higher than IASI one before the smoothing, but lower when the smoothing is taken into account.

For the MG dataset, we only report statistics of the direct comparison but we distinguish a case with all collocated measurements and another (bottom row in Table 1) with only the collocated retrievals which have similar degrees of freedom ($\text{DOFS}_{\text{IASI}} = \text{DOFS}_{\text{TES}} \pm 0.3$). When all the measurements are taken into account we find a SD of 46% in agreement with the theoretical error estimate. The correlation coefficient of 0.67 for this dataset is significantly higher than for the PIO dataset due to the larger amplitude of variations of δD along the meridional gradient (higher signal to noise ratio). The SD of the differences and the correlation coefficient are improved to 37% and 0.76 when only considering retrievals with similar degrees of freedom.

4.4.2 Systematic difference between IASI and TES

We calculate the mean bias for the 3–6 km layer as the mean difference between IASI and TES. We find a bias of +20% when using the non-smoothed data from PIO and MD datasets together and a bias of –3% when TES retrieval are smoothed with IASI averaging kernels (considering only collocated measurements where TES sensitivity is higher than IASI). The significant bias found for the non-smoothed data is probably due to the low vertical resolution of IASI. The averaging kernels indicate indeed that IASI is sensitive to a thicker layer of the atmosphere than TES which is likely to give a more enriched signal because of the mixing with information from the lowest layers. The bias when TES is smoothed according to IASI sensitivity is almost negligible. Although

this may appear an encouraging result it is also questioning as TES data V005 are bias corrected, for uncertainties in spectroscopic line strength (Herman et al., 2014; Worden et al., 2011). As we use the same spectroscopic parameters for IASI retrieval, the high level of agreement could suggest another origin than spectroscopy for the bias applied to TES δD .

4.5 Spatio-temporal variations of the δD – $\log(q)$ relation

For the MD dataset we analyse δD – q relations at 4.5 km from each instrument for bins of 10° , in terms of the correlation coefficient between δD and $\log(q)$ and the slope of the regression curve δD vs. $\log(q)$. The variations of these parameters along the meridional gradient are shown in Fig. 5. The 2 instruments present very coherent variations of the δD – q relation. We also see that for each instrument the correlation coefficient δD – q varies strongly with latitude. In the case of a perfect Rayleigh distillation, δD would have a correlation coefficient of 1 with $\log(q)$ (Eq. 11). The values found for TES and IASI are the closest to 1 at 5° S and significantly lower at other latitudes, indicating that processes different than Rayleigh distillation are at play.

With PIO dataset we investigate both spatial and temporal variations of the δD – q relation at 3.5 and 5.5 km. We distinguish 3 different areas each of 30° longitudes (from West to East: A, B and C) in the entire dataset and we also separate winter (DJF) from summer (JJA). The collocated pairs corresponding to these categories are plotted in Fig. 6. In this case, TES profiles (H_2O and δD) have been smoothed with IASI averaging kernels. We also plot the Rayleigh distillation curve (purple line) according to Eq. (11) with $q_0 = 3 \cdot 10^{-2} \text{ mol mol}^{-1}$ and $\delta D_0 = -70\%$ which determine a lower limit for Rayleigh processes occurring at these latitudes. Above this curve, Rayleigh processes for drier source term and mixing processes can explain the isotopic composition. Below, only depleting processes can be at the origin of the observed values.

At 5.5 km, the seasonal and longitudinal patterns observed by TES and IASI are very similar. In particular see that for zone A the difference between the high δD values in summer and low values in winter are very different than what is observed in zone B

Cross-validation of IASI/MetOp δD retrievals

J.-L. Lacour et al.

Title Page

Abstract

Introduction

Conclusions

References

Tables

Figures



Back

Close

Full Screen / Esc

Printer-friendly Version

Interactive Discussion



Cross-validation of IASI/MetOp δD retrievals

J.-L. Lacour et al.

Title Page

Abstract

Introduction

Conclusions

References

Tables

Figures



Back

Close

Full Screen / Esc

Printer-friendly Version

Interactive Discussion



and the retrieved δD between 3 and 6 km, and the results are reported in Table 2. We have subdivided the MD dataset in 2 different latitudinal groups according to the TES sensitivity: tropical observations located between 15° S and 15° N and subtropical to mid-latitudes observations located between 15 and 45° in both hemisphere. Note also that the comparison TES-LMDZ considers one TES observation vs. one LMDZ cell, and that this results in a worse agreement than previous studies that generally average TES observations over time and/or space.

For the PIO dataset the values found in Table 2 show that the comparison LMDZ vs. TES shows a better correlation coefficient (0.26) than for the LMDZ vs. IASI comparison (0.15). This is also true for the MD dataset at tropical latitudes with slightly higher correlation coefficient of 0.46 and 0.30 for TES and IASI respectively. In contrast, for the subtropical to mid-latitudes observations, we find a better correlation coefficient for the LMDZ vs. IASI comparison (0.42) compared to the LMDZ vs. TES comparison (0.30). The better agreement between LMDZ (reality) and IASI above 15° makes sense since we observe a significant decrease in TES sensitivity at these latitudes (see Fig. 3).

With the PIO dataset we finally investigate how the number of available observations can impact a model–instrument comparison. This is interesting because the number of daily IASI observations in one model cell ($3.75^\circ \times 2.53^\circ$) on a given day can be very large. Indeed, from the histogram in Fig. 7 we see that there is about 25% of the LMDZ cells that contains 1 to 10 observations and about 12% that contains 90 observations or more. The average number of observations available per cell is 46. The correlation coefficient between IASI and LMDZ increases compared to a one to one comparison, due on one hand, to the decrease of the observational error by \sqrt{N} when averaging several observations and on the other hand to the better sampling of the model cell by IASI that allows to capture the variability of δD within this cell. When including less than 10 observations the correlation coefficient is below 0.25 but it increases up to 0.5 when including more than 90 observations. This is important and suggests that model–observation comparison could be largely improved by exploiting the unprecedented sampling of IASI.

5.3 Expected difference

The expected differences for the direct IASI-FTIR comparison are calculated according to Eq. (8) in the same way as for TES comparisons. The same \mathbf{S}_c covariance matrix was also used. To evaluate the significance of the cross-validation, we compare the expected differences (black curve) in Fig. 9 at the three sites with the global δD variability (dark blue curve) but also with the regional variabilities (respectively green, brown and cyan curves for Kiruna, Karlsruhe and Izana). The variabilities were calculated from LMDZ model profiles within a given 20° latitudinal band. We can see from Fig. 9 that Kiruna and Karlsruhe present very similar error budgets mainly controlled by IASI observational error while at Izana the smoothing error also impacts the expected difference. For this comparison, we found that the smoothing of one instrument averaging kernels with the other was not productive. The comparison can thus not be optimized to take into account the different vertical sensitivities of the two instruments and only the direct comparison is discussed next.

The error difference budgets are shown in Fig. 9, representative of an average of the error budgets of a one month period. We note from Fig. 9 that the observational errors from the FTIR and from IASI are very different. For both sites the FTIR observational error is indeed lower than 20% throughout the vertical profile while IASI observational error ranges from 20% around 3–4 km to 80% in the upper troposphere. It is interesting here that the IASI observational error is significantly smaller in the lower troposphere compared to the error budget discussed previously in Fig. 4. This is mainly due to the fact that the two sites are on the continent, where the sensitivity of IASI to near surface δD is better due to more favourable thermal contrast. It is also interesting to notice that the IASI observational error in the lower troposphere does not exceed the δD variability at global scale and at a regional scale. This indicates that IASI retrievals provide relevant δD measurements in these conditions even in the boundary layer.

For Kiruna and Karlsruhe, the total expected difference is lowest in the free troposphere (about 20% for Kiruna and 35% for Karlsruhe) and highest in the upper

Cross-validation of IASI/MetOp δD retrievals

J.-L. Lacour et al.

Title Page

Abstract

Introduction

Conclusions

References

Tables

Figures



Back

Close

Full Screen / Esc

Printer-friendly Version

Interactive Discussion



troposphere. Compared to the regional expected variability of δD , the comparison might be considered useful below 5 km since both budgets show expected difference lower than the δD variability at regional level.

At Izana, the total expected difference ranges from 90‰ at 2.5 km to about 60‰ at 4.5 km. At higher altitude the total expected error exceeds the natural variability of δD . In this case it is not only the IASI observational error that dominates the total difference expected. From 2.5 to 4 km the smoothing error is indeed large and contributes with both IASI and FTIR observational error. From 4 to 6 km the FTIR observational error becomes less important while at higher altitude it is the IASI observational error that becomes predominant again. The comparison appears significant with respect to the variability of δD at global scale but not at regional scale.

5.4 Expected vs. real differences

The real difference between the 2 instruments are calculated as the SD of the difference for each level for the corresponding time period of the computed error budgets. As in the IASI vs. TES comparison the SD profiles are plotted (green curves) on the error budget in Fig. 9 for the three sites.

We find that the SD profiles of the difference follow well the error profiles expected from the theoretical error (although with small deviations at Karlsruhe and Izana). This indicates that the error budget and sensitivity characterization are realistic and correct.

5.5 Statistics of the agreement between FTIRs and IASI

Figure 10 gives a scatter plot of IASI vs. FTIR observations for the three different sites. The data refer to the δD at 2.5 km for Kiruna and Karlsruhe and at 5.5 km for Izana, which are the altitudes for which the two instruments share the most sensitivity. The SD of the difference between IASI and FTIR for all the collocated measurements are 24, 35 and 55‰ for Kiruna, Karlsruhe and Izana respectively which is in very good agreement with theoretical expected difference. The correlation coefficients of 0.75,

Cross-validation of IASI/MetOp δD retrievals

J.-L. Lacour et al.

Title Page

Abstract

Introduction

Conclusions

References

Tables

Figures



Back

Close

Full Screen / Esc

Printer-friendly Version

Interactive Discussion



panel). Since the different retrievals are not considering the same atmosphere this is a qualitative approach.

The extreme right panel of Fig. 11 shows that the three different sites exhibit very different distributions in the δD - $\log(q)$ space. The amplitude of variations are very similar for IASI and the ground-based FTIR. The variability is the largest at Izana with 400% between the minimum and maximum values, due to the fact that the retrieved value refer to the free troposphere (5.5 km) where the true variability is indeed expected to be large. The amplitude of variations is the lowest for Kiruna. At this site for which no winter collocated points were available, we observe a good agreement between the two distributions. The amplitudes of variations (for δD and H_2O) for both instruments are similar as well as the seasonal differences although in the case of IASI the seasonal patterns appear to be more scattered. At Karlsruhe the general patterns agree best despite a steeper slope for IASI and shows well differentiated seasonal differences for both instruments. At Izana IASI retrievals are more scattered than the FTIR ones owing to the larger observational error from IASI.

Overall Fig. 11 shows that IASI and the ground-based FTIR reproduce similar spatial and seasonal variations in humidity- δD relationships. We can safely conclude that the two instruments probe the same hydrological processes in the same way.

6 Conclusions

In this study we have cross-validated δD profiles retrieved from IASI spectra with profiles from TES and three ground-based FTIRs. We provided a comprehensive and detailed estimation of error differences expected from the comparisons between the different instruments. Generally, we find that the total difference between TES and IASI, and between IASI and the ground-based FTIR is controlled by IASI observational error and by the smoothing error due to the differences in sensitivity of the instruments. In the comparison with the ground-based FTIRs, only a direct comparison was performed because it was not possible to simulate one retrieval with the averaging kernels of the

Cross-validation of IASI/MetOp δD retrievals

J.-L. Lacour et al.

Title Page

Abstract

Introduction

Conclusions

References

Tables

Figures



Back

Close

Full Screen / Esc

Printer-friendly Version

Interactive Discussion



model evaluation against observations could be optimized with IASI more than with other sounders (in the free troposphere).

Appendix A: Sensitivity change along the meridional gradient for IASI retrieval

Since IASI presents some sensitivity to surface we expect a change in sensitivity with decreasing surface temperature. This change is not visible on Fig. 3, in this appendix we further investigate this apparent contradiction. In Fig. A1, we used all available IASI data along the meridional gradient and average the degrees of freedom for H₂O and δD on latitude bins. For H₂O there is an increase in sensitivity with surface temperature and a small decrease is observed with high water vapour content. For δD we also observe a significant increase in DOFS with latitude but with a more significant drop off in sensitivity with high water vapour content. This could explain why IASI sensitivity is more constant with latitudinal variations than TES.

Acknowledgements. IASI has been developed and built under the responsibility of the “Centre National d’Etudes Spatiales” (CNES, France). It is flown on-board the Metop satellites as part of the EUMETSAT Polar System. The IASI L1 data are received through the EUMETCast near real-time data distribution service. The research in Belgium was funded by the F.R.S.-FNRS, the Belgian State Federal Office for Scientific, Technical and Cultural Affairs (Prodex arrangement 4000111403 IASI.FLOW). L. Clarisse and P-F. Coheur are respectively Research Associate (Chercheur Qualifié) and Senior Research Associate (Maître de Recherches) with F.R.S.-FNRS. C. Clerbaux is grateful to CNES for scientific collaboration and financial support. The ground-based FTIR retrievals have been performed in the framework of the project MUSICA, which is funded by the European Research Council under the European Community’s Seventh Framework Programme (FP7/2007-2013)/ERC Grant agreement number 256961.

Cross-validation of IASI/MetOp δD retrievals

J.-L. Lacour et al.

Title Page

Abstract

Introduction

Conclusions

References

Tables

Figures



Back

Close

Full Screen / Esc

Printer-friendly Version

Interactive Discussion



References

- Allan, R. P., Ringer, M. A., and Slingo, A.: Evaluation of moisture in the Hadley Centre climate model using simulations of HIRS water-vapour channel radiances, *Q. J. Roy. Meteor. Soc.*, 129, 3371–3389, doi:10.1256/qj.02.217, 2003. 11089
- 5 Bates, J. J. and Jackson, D. L.: A comparison of water vapor observations with AMIP1 simulations, *J. Geophys. Res.*, 102, 21837–21852, doi:10.1029/97JD01769, 1997. 11089
- Beer, R., Glavich, T. A., and Rider, D. M.: Tropospheric emission spectrometer for the Earth Observing System's Aura satellite, *Appl. Optics*, 40, 2356–2367, 2001. 11099
- 10 Boesch, H., Deutscher, N. M., Warneke, T., Byckling, K., Cogan, A. J., Griffith, D. W. T., Notholt, J., Parker, R. J., and Wang, Z.: HDO/H₂O ratio retrievals from GOSAT, *Atmos. Meas. Tech.*, 6, 599–612, doi:10.5194/amt-6-599-2013, 2013. 11090
- Brogniez, H. and Pierrehumbert, R. T.: Intercomparison of tropical tropospheric humidity in GCMs with AMSU-B water vapor data, *Geophys. Res. Lett.*, 34, L17812, doi:10.1029/2006GL029118, 2007. 11089
- 15 Calisesi, Y., Soebijanta, V. T., and van Oss, R.: Regridding of remote soundings: formulation and application to ozone profile comparison, *J. Geophys. Res.*, 110, D23306, doi:10.1029/2005JD006122, 2005. 11093, 11094
- Ceccherini, S., Carli, B., Pascale, E., Prosperi, M., Raspollini, P., and Dinelli, B. M.: Comparison of measurements made with two different instruments of the same atmospheric vertical profile, *Appl. Optics*, 42, 6465–6473, doi:10.1364/AO.42.006465, 2003. 11094
- 20 Cess, R. D., Potter, G. L., Blanchet, J. P., Boer, G. J., Del Genio, A. D., Déqué, M., Dymnikov, V., Galin, V., Gates, W. L., Ghan, S. J., Kiehl, J. T., Lacis, A. A., Le Treut, H., Li, Z.-X., Liang, X.-Z., McAvaney, B. J., Meleshko, V. P., Mitchell, J. F. B., Morcrette, J.-J., Randall, D. A., Rikus, L., Roeckner, E., Royer, J. F., Schlese, U., Sheinin, D. A., Slingo, A., Sokolov, A. P., Taylor, K. E.,
- 25 Washington, W. M., Wetherald, R. T., Yagai, I., and Zhang, M.-H.: Intercomparison and interpretation of climate feedback processes in 19 atmospheric general circulation models, *J. Geophys. Res.*, 95, 16601–16615, doi:10.1029/JD095iD10p16601, 1990. 11089
- Clerbaux, C., Boynard, A., Clarisse, L., George, M., Hadji-Lazaro, J., Herbin, H., Hurtmans, D., Pommier, M., Razavi, A., Turquety, S., Wespes, C., and Coheur, P.-F.: Monitoring of atmospheric composition using the thermal infrared IASI/MetOp sounder, *Atmos. Chem. Phys.*, 9, 6041–6054, doi:10.5194/acp-9-6041-2009, 2009. 11090, 11098
- 30

Cross-validation of IASI/MetOp δD retrievals

J.-L. Lacour et al.

[Title Page](#)[Abstract](#)[Introduction](#)[Conclusions](#)[References](#)[Tables](#)[Figures](#)[Back](#)[Close](#)[Full Screen / Esc](#)[Printer-friendly Version](#)[Interactive Discussion](#)

Cross-validation of IASI/MetOp δD retrievals

J.-L. Lacour et al.

Title Page

Abstract

Introduction

Conclusions

References

Tables

Figures



Back

Close

Full Screen / Esc

Printer-friendly Version

Interactive Discussion



- Craig, H.: Isotopic variations in meteoric waters, *Science*, 133, 1702–1703, doi:10.1126/science.133.3465.1702, 1961. 11089
- de F. Forster, P. and Collins, M.: Quantifying the water vapour feedback associated with post-Pinatubo global cooling, *Clim. Dynam.*, 23, 207–214, doi:10.1007/s00382-004-0431-z, 2004. 11089
- Draxler, R. R. and Hess, G. D.: An overview of the HYSPLIT4 modeling system for trajectories, dispersion and deposition, *Aust. Meteorol. Mag.*, 47, 295–308, 1998. 11101
- Dufresne, J.-L. and Bony, S.: An assessment of the primary sources of spread of global warming estimates from coupled atmosphere? Ocean models, *J. Climate*, 21, 5135–5144, doi:10.1175/2008JCLI2239.1, 2008. 11089
- Frankenberg, C., Yoshimura, K., Warneke, T., Aben, I., Butz, A., Deutscher, N., Griffith, D., Hase, F., Notholt, J., Schneider, M., Schrijver, H., and Rockmann, T.: Dynamic processes governing lower-tropospheric HDO / H₂O ratios as observed from space and ground, *Science*, 325, 1374–1377, doi:10.1126/science.1173791, 2009. 11090
- Frankenberg, C., Wunch, D., Toon, G., Risi, C., Scheepmaker, R., Lee, J.-E., Wennberg, P., and Worden, J.: Water vapor isotopologue retrievals from high-resolution GOSAT shortwave infrared spectra, *Atmos. Meas. Tech.*, 6, 263–274, doi:10.5194/amt-6-263-2013, 2013. 11090
- Galewsky, J., Strong, M., and Sharp, Z. D.: Measurements of water vapor D/H ratios from Mauna Kea, Hawaii, and implications for subtropical humidity dynamics, *Geophys. Res. Lett.*, 34, L22808, doi:10.1029/2007GL031330, 2007. 11097
- Herman, R. L., Cherry, J. E., Young, J., Welker, J. M., Noone, D., Kulawik, S. S., and Worden, J.: Aircraft validation of Aura Tropospheric Emission Spectrometer retrievals of HDO/H₂O, *Atmos. Meas. Tech.*, 7, 3127–3138, doi:10.5194/amt-7-3127-2014, 2014. 11090, 11099, 11106
- Hilton, F., Armante, R., August, T., Barnet, C., Bouchard, A., Camy-Peyret, C., Capelle, V., Clarisse, L., Clerbaux, C., Coheur, P.-F., Collard, A., Crevoisier, C., Dufour, G., Edwards, D., Fajjan, F., Fourrié, N., Gambacorta, A., Goldberg, M., Guidard, V., Hurtmans, D., Illingworth, S., Jacquinet-Husson, N., Kerzenmacher, T., Klaes, D., Lavanant, L., Masiello, G., Matricardi, M., McNally, A., Newman, S., Pavelin, E., Payan, S., Péquignot, E., Peyridieu, S., Phulpin, T., Remedios, J., Schlüssel, P., Serio, C., Strow, L., Stubenrauch, C., Taylor, J., Tobin, D., Wolf, W., and Zhou, D.: Hyperspectral earth observation from IASI: five years of accomplishments, *B. Am. Meteorol. Soc.*, 93, 347–370, doi:10.1175/BAMS-D-11-00027.1, 2012. 11098

Cross-validation of IASI/MetOp δD retrievals

J.-L. Lacour et al.

[Title Page](#)
[Abstract](#)
[Introduction](#)
[Conclusions](#)
[References](#)
[Tables](#)
[Figures](#)




[Back](#)
[Close](#)
[Full Screen / Esc](#)
[Printer-friendly Version](#)
[Interactive Discussion](#)


- Hurtmans, D., Coheur, P.-F., Wespes, C., Clarisse, L., Scharf, O., Clerbaux, C., Hadji-Lazaro, J., George, M., and Turquety, S.: FORLI radiative transfer and retrieval code for IASI, *J. Quant. Spectrosc. Ra.*, 113, 1391–1408, doi:10.1016/j.jqsrt.2012.02.036, 2012. 11100
- Lacour, J.-L., Risi, C., Clarisse, L., Bony, S., Hurtmans, D., Clerbaux, C., and Coheur, P.-F.: Mid-tropospheric δD observations from IASI/MetOp at high spatial and temporal resolution, *Atmos. Chem. Phys.*, 12, 10817–10832, doi:10.5194/acp-12-10817-2012, 2012. 11090, 11091, 11092, 11098, 11101, 11107
- Noone, D.: Pairing measurements of the water vapor isotope ratio with humidity to deduce atmospheric moistening and dehydration in the tropical mid-troposphere, *J. Climate*, 25, 4476–4494, doi:10.1175/JCLI-D-11-00582.1, 2012. 11089, 11097
- Noone, D., Galewsky, J., Sharp, Z. D., Worden, J., Barnes, J., Baer, D., Bailey, A., Brown, D. P., Christensen, L., Crosson, E., Dong, F., Hurley, J. V., Johnson, L. R., Strong, M., Toohey, D., Van Pelt, A., and Wright, J. S.: Properties of air mass mixing and humidity in the subtropics from measurements of the D/H isotope ratio of water vapor at the Mauna Loa Observatory, *J. Geophys. Res.*, 116, D22113, doi:10.1029/2011JD015773, 2011. 11097
- Pierce, D. W., Barnett, T. P., Fetzer, E. J., and Gleckler, P. J.: Three-dimensional tropospheric water vapor in coupled climate models compared with observations from the AIRS satellite system, *Geophys. Res. Lett.*, 33, L21701, doi:10.1029/2006GL027060, 2006. 11089
- Pierrehumbert, R. T., Brogniez, H., and Roca, R.: *On the Relative Humidity of the Earth's Atmosphere*, Princeton University Press, Princeton, NJ, 2007. 11089
- Pommier, M., Lacour, J.-L., Risi, C., Bréon, F. M., Clerbaux, C., Coheur, P.-F., Griбанov, K., Hurtmans, D., Jouzel, J., and Zakharov, V.: Observation of tropospheric δD by IASI over western Siberia: comparison with a general circulation model, *Atmos. Meas. Tech.*, 7, 1581–1595, doi:10.5194/amt-7-1581-2014, 2014. 11107, 11109
- Rayleigh, L.: On the distillation of binary mixtures, *Philos. Mag.*, 4, 521–537, 1902. 11097
- Risi, C., Bony, S., and Vimeux, F.: Influence of convective processes on the isotopic composition of precipitation and water vapor in the tropics: 2. Physical interpretation of the amount effect, *J. Geophys. Res.*, 113, D19306, doi:10.1029/2008JD009943, 2008. 11097
- Risi, C., Bony, S., Vimeux, F., and Jouzel, J.: Water-stable isotopes in the LMDZ4 general circulation model: model evaluation for present-day and past climates and applications to climatic interpretations of tropical isotopic records, *J. Geophys. Res.*, 115, D12118, doi:10.1029/2009JD013255, 2010. 11096, 11107

Cross-validation of IASI/MetOp δD retrievals

J.-L. Lacour et al.

Title Page

Abstract

Introduction

Conclusions

References

Tables

Figures



Back

Close

Full Screen / Esc

Printer-friendly Version

Interactive Discussion



Risi, C., Noone, D., Worden, J., Frankenberg, C., Stiller, G., Kiefer, M., Funke, B., Walker, K., Bernath, P., Schneider, M., Bony, S., Lee, J., Brown, D., and Sturm, C.: Process-evaluation of tropospheric humidity simulated by general circulation models using water vapor isotopic observations: 2. Using isotopic diagnostics to understand the mid and upper tropospheric moist bias in the tropics and subtropics, *J. Geophys. Res.*, 117, D05304, doi:10.1029/2011JD016623, 2012a. 11089

Risi, C., Noone, D., Worden, J., Frankenberg, C., Stiller, G., Kiefer, M., Funke, B., Walker, K., Bernath, P., Schneider, M., Wunch, D., Sherlock, V., Deutscher, N., Griffith, D., Wennberg, P. O., Strong, K., Smale, D., Mahieu, E., Barthlott, S., Hase, F., Garcia, O., Notholt, J., Warneke, T., Toon, G., Sayres, D., Bony, S., Lee, J., Brown, D., Uemura, R., and Sturm, C.: Process-evaluation of tropospheric humidity simulated by general circulation models using water vapor isotopologues: 1. Comparison between models and observations, *J. Geophys. Res.*, 117, D05303, doi:10.1029/2011JD016621, 2012b. 11089, 11090, 11091, 11096, 11107

Rodgers, C. D.: *Inverse Methods for Atmospheric Sounding: Theory and Practise*, World Scientific, 2000. 11093, 11107

Rodgers, C. D. and Connor, B. J.: Intercomparison of remote sounding instruments, *J. Geophys. Res.*, 108, 4116, doi:10.1029/2002JD002299, 2003. 11090, 11091, 11095, 11096

Samuels-Crow, K. E., Galewsky, J., Hardy, D. R., Sharp, Z. D., Worden, J., and Braun, C.: Upwind convective influences on the isotopic composition of atmospheric water vapor over the tropical Andes, *J. Geophys. Res.-Atmos.*, 119, 7051–7063, doi:10.1002/2014JD021487, 2014. 11089

Schneider, M. and Hase, F.: Optimal estimation of tropospheric H_2O and δD with IASI/METOP, *Atmos. Chem. Phys.*, 11, 11207–11220, doi:10.5194/acp-11-11207-2011, 2011. 11090, 11091, 11098

Schneider, M., Hase, F., and Blumenstock, T.: Ground-based remote sensing of HDO/ H_2O ratio profiles: introduction and validation of an innovative retrieval approach, *Atmos. Chem. Phys.*, 6, 4705–4722, doi:10.5194/acp-6-4705-2006, 2006. 11092

Schneider, M., Barthlott, S., Hase, F., González, Y., Yoshimura, K., García, O. E., Sepúlveda, E., Gomez-Pelaez, A., Gisi, M., Kohlhepp, R., Dohe, S., Blumenstock, T., Wiegele, A., Christner, E., Strong, K., Weaver, D., Palm, M., Deutscher, N. M., Warneke, T., Notholt, J., Lejeune, B., Demoulin, P., Jones, N., Griffith, D. W. T., Smale, D., and Robinson, J.: Ground-based remote sensing of tropospheric water vapour isotopologues within the project MUSICA,

**Cross-validation of
IASI/MetOp δ D
retrievals**

J.-L. Lacour et al.

Title Page

Abstract

Introduction

Conclusions

References

Tables

Figures



Back

Close

Full Screen / Esc

Printer-friendly Version

Interactive Discussion



Atmos. Meas. Tech., 5, 3007–3027, doi:10.5194/amt-5-3007-2012, 2012. 11091, 11092, 11093, 11097, 11099, 11101

Schneider, M., González, Y., Dyroff, C., Christner, E., Wiegele, A., Barthlott, S., García, O. E., Sepúlveda, E., Hase, F., Andrey, J., Blumenstock, T., Guirado, C., Ramos, R., and Rodríguez, S.: Empirical validation and proof of added value of MUSICA's tropospheric δ D remote sensing products, Atmos. Meas. Tech. Discuss., 7, 6917–6969, doi:10.5194/amt-d-7-6917-2014, 2014. 11090, 11097, 11112

Sherwood, S. C., Roca, R., Weckwerth, T. M., and Andronova, N. G.: Tropospheric water vapor, convection, and climate, Rev. Geophys., 48, RG2001, doi:10.1029/2009RG000301, 2010. 11089

Sherwood, S. C., Bony, S., and Dufresne, J.-L.: Spread in model climate sensitivity traced to atmospheric convective mixing, Nature, 505, 37–42, doi:10.1038/nature12829, 2014. 11089

Soden, B. J. and Bretherton, F. P.: Evaluation of water vapor distribution in general circulation models using satellite observations, J. Geophys. Res., 99, 1187–1210, doi:10.1029/93JD02912, 1994. 11089

Soden, B. J. and Held, I. M.: An assessment of climate feedbacks in coupled ocean atmosphere models, J. Climate, 19, 3354–3360, doi:10.1175/JCLI3799.1, 2006. 11089

Strong, M., Sharp, Z. D., and Gutzler, D. S.: Diagnosing moisture transport using D/H ratios of water vapor, Geophys. Res. Lett., 34, L03404, doi:10.1029/2006GL028307, 2007. 11089

von Clarmann, T.: Validation of remotely sensed profiles of atmospheric state variables: strategies and terminology, Atmos. Chem. Phys., 6, 4311–4320, doi:10.5194/acp-6-4311-2006, 2006. 11090

Wiegele, A., Schneider, M., Hase, F., Barthlott, S., García, O. E., Sepúlveda, E., González, Y., Blumenstock, T., Raffalski, U., Gisi, M., and Kohlhepp, R.: The MUSICA MetOp/IASI H_2O and δ D products: characterisation and long-term comparison to NDACC/FTIR data, Atmos. Meas. Tech., 7, 2719–2732, doi:10.5194/amt-7-2719-2014, 2014. 11090, 11097, 11100, 11112

Worden, J., Bowman, K., Noone, D., Beer, R., Clough, S., Eldering, A., Fisher, B., Goldman, A., Gunson, M., Herman, R., Kulawik, S. S., Lampel, M., Luo, M., Osterman, G., Rinsland, C., Rodgers, C., Sander, S., Shephard, M., and Worden, H.: Tropospheric Emission Spectrometer observations of the tropospheric HDO / H_2O ratio: estimation approach and characterization, J. Geophys. Res., 111, D16309, doi:10.1029/2005JD006606, 2006. 11092

Cross-validation of IASI/MetOp δD retrievals

J.-L. Lacour et al.

Title Page

Abstract

Introduction

Conclusions

References

Tables

Figures

◀

▶

◀

▶

Back

Close

Full Screen / Esc

Printer-friendly Version

Interactive Discussion



Worden, J., Noone, D., and Bowman, K.: Importance of rain evaporation and continental convection in the tropical water cycle, *Nature*, 445, 528–532, doi:10.1038/nature05508, 2007. 11089, 11090, 11097

Worden, J., Noone, D., Galewsky, J., Bailey, A., Bowman, K., Brown, D., Hurley, J., Kulawik, S., Lee, J., and Strong, M.: Estimate of bias in Aura TES HDO/H₂O profiles from comparison of TES and in situ HDO/H₂O measurements at the Mauna Loa observatory, *Atmos. Chem. Phys.*, 11, 4491–4503, doi:10.5194/acp-11-4491-2011, 2011. 11106

Worden, J., Kulawik, S., Frankenberg, C., Payne, V., Bowman, K., Cady-Peirara, K., Wecht, K., Lee, J.-E., and Noone, D.: Profiles of CH₄, HDO, H₂O, and N₂O with improved lower tropospheric vertical resolution from Aura TES radiances, *Atmos. Meas. Tech.*, 5, 397–411, doi:10.5194/amt-5-397-2012, 2012. 11091, 11092, 11099

Yoshimura, K., Frankenberg, C., Lee, J., Kanamitsu, M., Worden, J., and Röckmann, T.: Comparison of an isotopic atmospheric general circulation model with new quasi-global satellite measurements of water vapor isotopologues, *J. Geophys. Res.*, 116, D19118, doi:10.1029/2011JD016035, 2011. 11107

**Cross-validation of
IASI/MetOp δD
retrievals**

J.-L. Lacour et al.

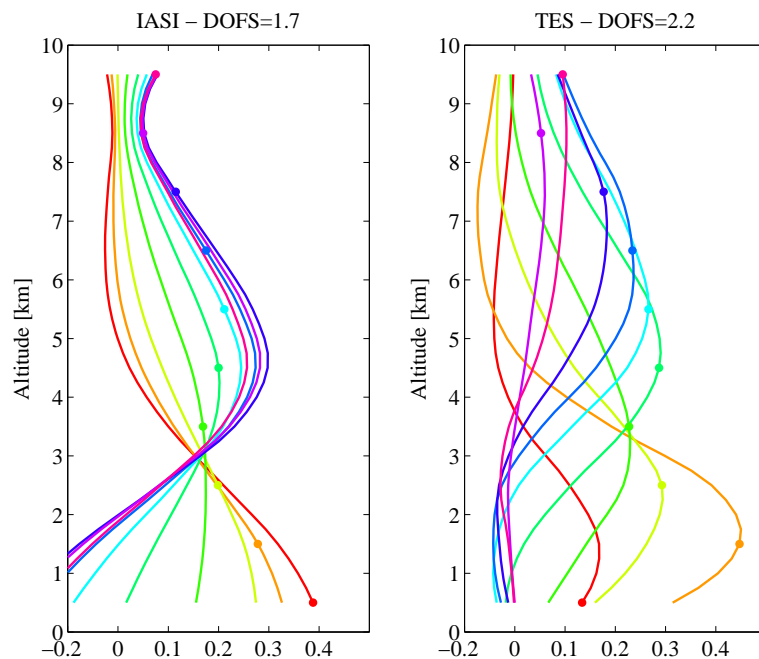
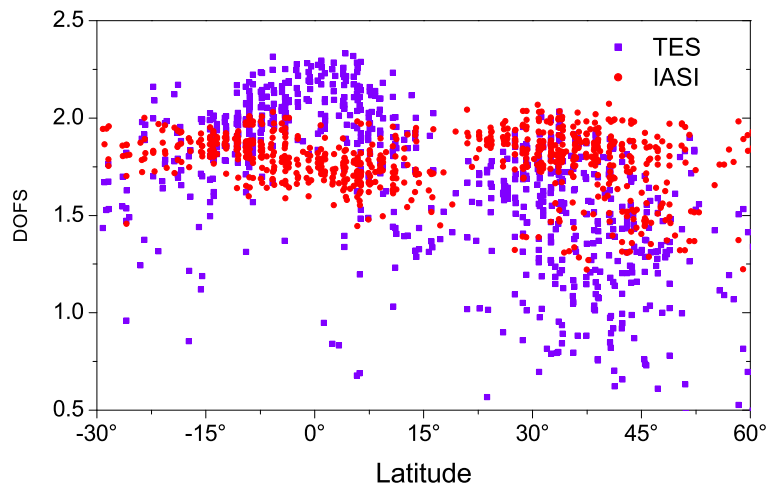


Figure 2. Typical averaging kernels in $\{\delta D\}$ proxy space for IASI (left panel) and for TES (right panel) for a tropical scene (2.5° N). The nominal heights of the kernels are marked by filled circles.

[Title Page](#)[Abstract](#)[Introduction](#)[Conclusions](#)[References](#)[Tables](#)[Figures](#)[◀](#)[▶](#)[◀](#)[▶](#)[Back](#)[Close](#)[Full Screen / Esc](#)[Printer-friendly Version](#)[Interactive Discussion](#)

**Cross-validation of
IASI/MetOp δD
retrievals**

J.-L. Lacour et al.

**Figure 3.** TES (purple) and IASI (red) degrees of freedom for δD along the meridional gradient.

Title Page

Abstract

Introduction

Conclusions

References

Tables

Figures



Back

Close

Full Screen / Esc

Printer-friendly Version

Interactive Discussion



Cross-validation of IASI/MetOp δD retrievals

J.-L. Lacour et al.

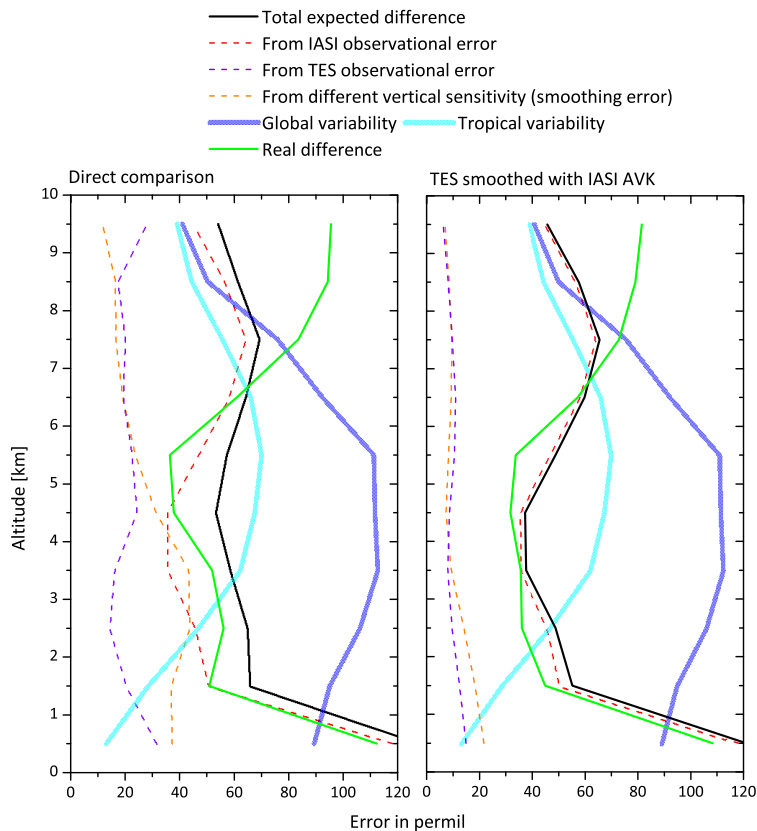


Figure 4. Expected difference of the IASI and TES retrieval at tropical latitudes and its different contribution sources according to Eq. (8) for the direct comparison (left) and to Eq. (10) for the smoothed comparison (right). The squareroot of the diagonal elements of the \mathbf{S}_δ matrix as well as the different contribution matrices are plotted. Real differences are also shown in green.

**Cross-validation of
IASI/MetOp δD
retrievals**

J.-L. Lacour et al.

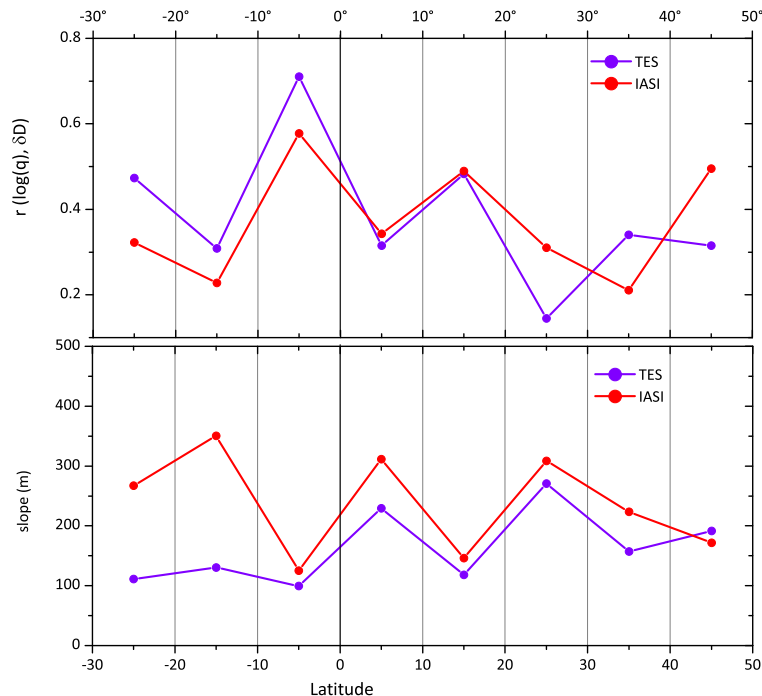


Figure 5. Top panel: variation of the correlation coefficient between $\log(q)$ and δD at 4.5 km along the meridional gradient for TES (purple) and IASI (red). Bottom panel: variation of the slope of the linear regression between $\log(q)$ and δD (spatial and temporal variability within the 10° bin) along the meridional gradient for TES (purple) and IASI (red).

Cross-validation of IASI/MetOp δD retrievals

J.-L. Lacour et al.

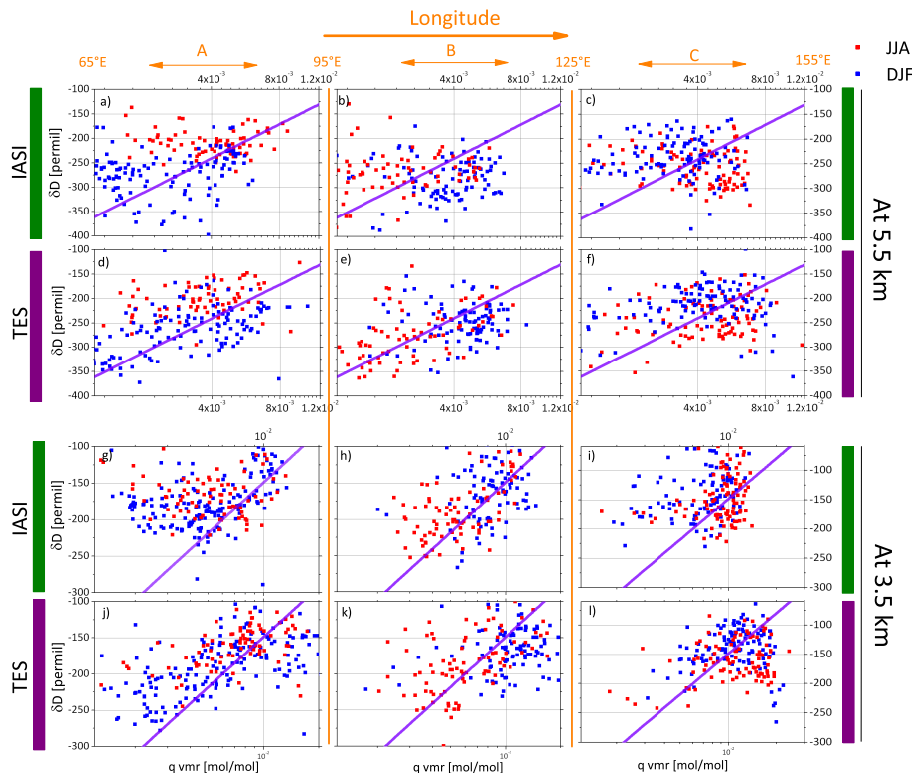


Figure 6. Spatio temporal variations of the δD – q relation for the PIO dataset. Retrieved δD and q are separated in 3 longitudinal boxes of 30° (A, B, C) from 65 to 155° E to highlight spatial variations. Winter (DJF, blue squares) and summer (JJA, red squares) are also separated to highlight seasonal variations. (a–c) correspond to IASI retrieved values at 5.5 km, and (g–i) to IASI retrieved values at 3.5 km. (d–f) correspond to TES retrieved values at 5.5 km, and (j–l) to TES retrieved values at 3.5 km. The purple line represents a Rayleigh distillation curve computed according to Eq. (11) with $q_0 = 0.03 \text{ mol mol}^{-1}$ and $\delta D_0 = -70\text{‰}$.

Title Page

Abstract Introduction

Conclusions References

Tables Figures

◀ ▶

◀ ▶

Back Close

Full Screen / Esc

Printer-friendly Version

Interactive Discussion



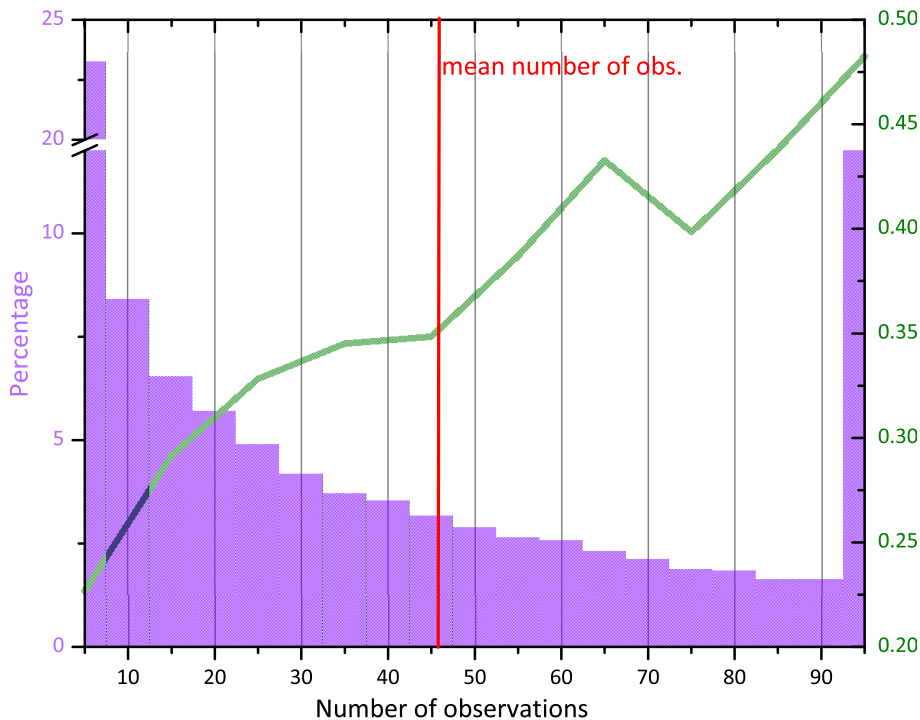


Figure 7. On the background (purple): histogram in percent of the number of IASI observations available per model cell for the LMDZ-IASI comparison (daily values) above the Pacific and Indian oceans dataset. In green, correlation coefficient between δD simulated by LMDZ and averaged δD from all observations available in the cell in function of the number of observations available.

Cross-validation of IASI/MetOp δD retrievals

J.-L. Lacour et al.

Title Page

Abstract

Introduction

Conclusions

References

Tables

Figures

◀

▶

◀

▶

Back

Close

Full Screen / Esc

Printer-friendly Version

Interactive Discussion



Cross-validation of IASI/MetOp δD retrievals

J.-L. Lacour et al.

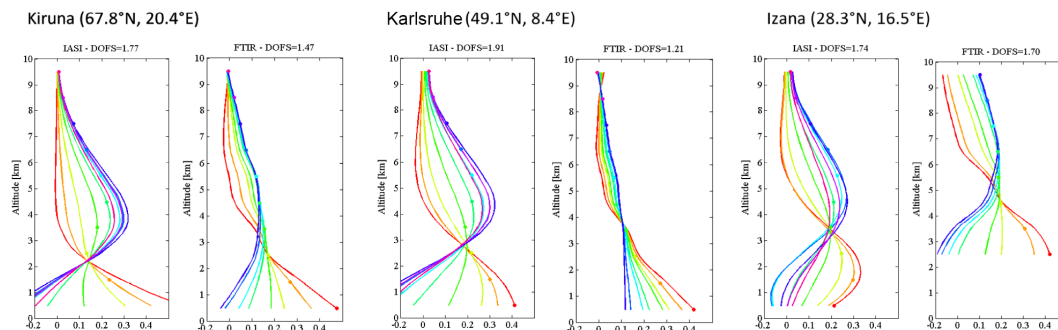


Figure 8. Averaging kernels in $\{\delta D\}$ proxy space for the three different sites of the comparison: (a) and (b) for Kiruna, (c) and (d) for Karlsruhe and (e) and (f) for Izana. (a), (c) and (e) corresponding to IASI and (b), (d) and (f) to the ground-based FTIR.

Title Page

Abstract

Introduction

Conclusions

References

Tables

Figures



Back

Close

Full Screen / Esc

Printer-friendly Version

Interactive Discussion



Cross-validation of IASI/MetOp δD retrievals

J.-L. Lacour et al.

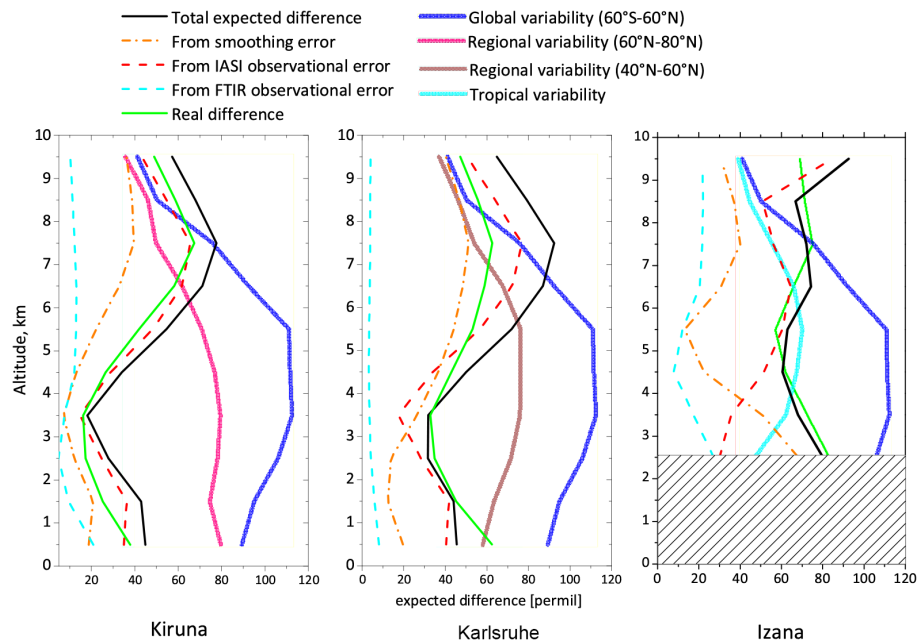


Figure 9. Same as Fig. 5 but for the comparison between IASI and the ground-based FTIR of Kiruna (left) and Karlsruhe (right).

Title Page

Abstract

Introduction

Conclusions

References

Tables

Figures

◀

▶

◀

▶

Back

Close

Full Screen / Esc

Printer-friendly Version

Interactive Discussion



**Cross-validation of
IASI/MetOp δD
retrievals**

J.-L. Lacour et al.

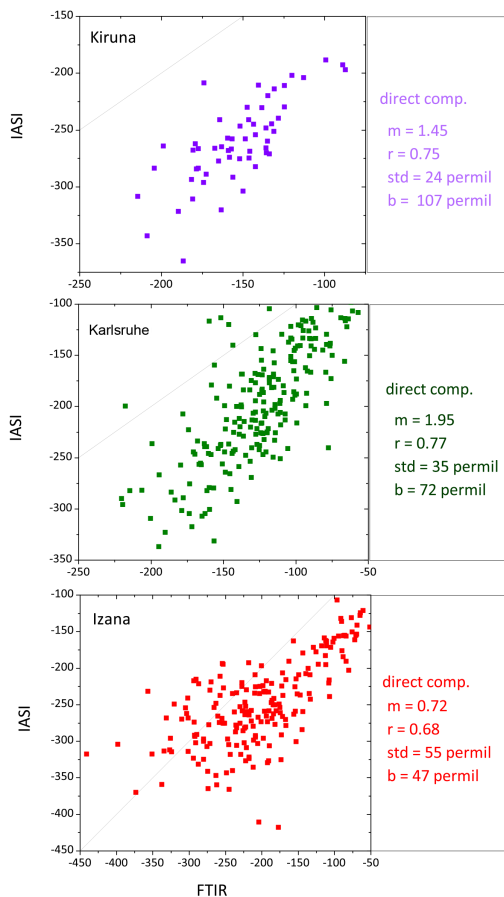


Figure 10. Scatter plot of IASI vs. FTIR δD from top to bottom for Kiruna (2.5 km), Karlsruhe (2.5 km) and Izana (5.5 km). We give the slopes of the major axis regression curves (m), the Pearson correlation coefficient (r), the SD of the difference and the mean bias (b , FTIR-IASI).

[Title Page](#)[Abstract](#)[Introduction](#)[Conclusions](#)[References](#)[Tables](#)[Figures](#)[Back](#)[Close](#)[Full Screen / Esc](#)[Printer-friendly Version](#)[Interactive Discussion](#)

Cross-validation of IASI/MetOp δD retrievals

J.-L. Lacour et al.

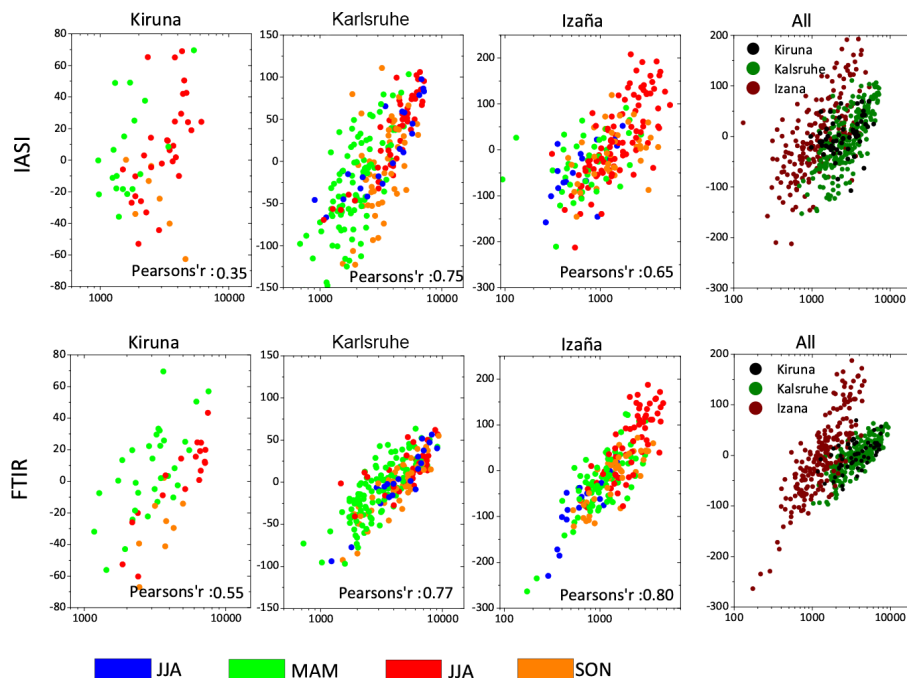


Figure 11. Distributions of IASI (top) and FTIR (bottom) observations in the $\log(q)$ – δD space for the three different sites (from left to right: Kiruna, Karlsruhe and Izaña). The colours refer to seasons. Distributions for the three sites together are given on the right panel, with colours differentiating the sites: brown is for Izaña, green for Karlsruhe and yellow for Kiruna. δD values are presented in relative variations. Pearson correlation coefficient between δD and $\log(q)$ are also documented in the bottom of the plots.

Cross-validation of IASI/MetOp δD retrievals

J.-L. Lacour et al.

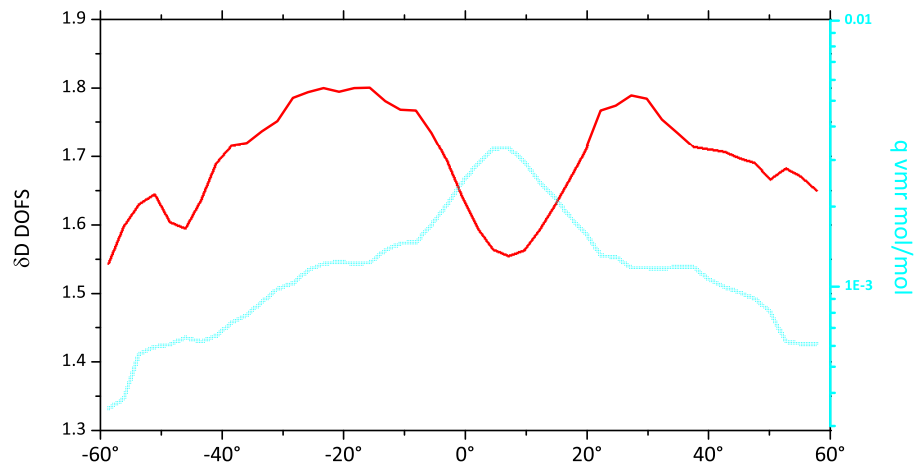


Figure A1. Variation of the degrees of freedom for IASI δD retrieval along the latitudinal gradient (red) and mixing ratio of water vapour at 4.5 km.

[Title Page](#)[Abstract](#)[Introduction](#)[Conclusions](#)[References](#)[Tables](#)[Figures](#)[◀](#)[▶](#)[◀](#)[▶](#)[Back](#)[Close](#)[Full Screen / Esc](#)[Printer-friendly Version](#)[Interactive Discussion](#)